Research Square

Preprints are preliminary reports that have not undergone peer review.
They should not be considered conclusive, used to inform clinical practice,
or referenced by the media as validated information.

Design and Characterization of Formazonate Transition Metal Complexes for Emerging Optoelectronic Applications

Pravendra Kumar
M J P Rohilkhand University
Brijesh Kumar
M J P Rohilkhand University
Sushmita Gupta
drsushmitagupta12@gmail.com
M J P Rohilkhand University
Prashant Kumar Pal
M J P Rohilkhand University

Research Article

Keywords: Formazonate, Sensitizer, Photodetector, chromophore

Posted Date: August 6th, 2026

DOI: https://doi.org/10.21203/rs.3.rs-10496546/v1

License: This work is licensed under a Creative Commons Attribution 4.0 International License.
Read Full License

Additional Declarations: No competing interests reported.

Abstract

Formazans are well known for their distinctive nitrogen backbone, vibrant coloration, and diverse applications in medicine. They also got recognition as an excellent optoelectronic material due to their intense visible-light absorption, structural versatility, and redox properties. He we synthesized formazonate and diphenyl amine metal complexes and investigated their structural, thermal and optical properties for potential photovoltaic applications. The structural study specifically underlined Co(II), Fe(II), and Cu(II) complexes with the general formula $[M_2A_2B_2]$, where **A** represents the bidentate formazonate ligand and **B** signifies the monodentate diphenyl amine ligand. In-depth spectroscopic analysis reveals these complexes possess a low band gap and consistent size distribution along with notable thermal stability. Tauc plot analysis showed an indirect band gap of 2.0 to 3.0 eV. The findings underscore the viability of these complexes for applications in semiconductor electronics as photodetectors, sensitizers and in photocatalytic activity. Due to low current generation at anode, they are suitable for dye-sensitized photodetectors as well as photo-catalytic hydrogen generation reaction.

1. Introduction

In the age of advanced electronic devices, there is surge to discover novel molecular materials suitable for such applications [1]. The photodetectors [2] have special attention because of their wide spread applications [3] in to optoelectronic devices, communication system, medical diagnostics and imaging [4]. They can detect light and convert it into electrical signal (relative voltage/current). Among various type of photodetectors, the photodiode detectors [5] are mostly used for optical communication technologies. Photodiode detectors are typically operating under reverse bias for fast response and high sensitivity. Common types include p-n, PIN, and avalanche photodiodes, each offering distinct advantages in terms of quantum efficiency, gain, and noise characteristics. These detectors have low dark current with fast response time under broad spectral range [6]. Photodiodes are widely used in optical communication, sensing, and imaging applications due to their linear response and reliability. Graphene is a high-speed photodetector [7] but it's photo responsivity is low. The MoS_2, GaS and GaSe have been reported as dye sensitized photo detectors with better photoresponse [8, 9]. Heterojunction of In-Se/b-Ga_2O_3, Ge-Se/violet phosphorous(GeSe/VP) and Graphene/$SrTiO_3$ have reported for good performance as low dark current type photodetectors [10–11].

Formazans constitute an important class of nitrogen-rich, highly conjugated chromophores characterized by the –N = N–C = N–NH– backbone, which imparts intense coloration and notable redox activity [12]. Since their first report by Nineham et. al. in the late 19th century, these compounds have attracted sustained attention due to their versatile chemical behavior and wide applicability [13–15]. Redox property of formazan extensively exploited in electrochemical and biological assays [16]. Their absorption maxima, typically spanning 300–650 nm, can be finely tuned through substitution with electron-donating or electron-withdrawing groups, making them suitable for optoelectronic and sensing applications. Deprotonated formazans (formazonates) act as effective bidentate chelating ligands, stabilizing a variety of transition metal ions through N,N-coordination [17–19]. The resulting complexes

are generally thermodynamically stable and exhibit enhanced electronic delocalization, leading to intense coloration and improved functional properties [20, 21]. Diphenylamine (DPA), an aromatic amine with a conjugated biphenyl framework, further complements this system as a versatile ligand [22]. Its electron-rich nitrogen center facilitates strong σ-donation, while the extended π-system enables weak π-back bonding interactions with metal centers [23]. This dual interaction enhances complex stability and promotes charge transfer processes. The combined use of formazan and diphenylamine ligands often leads to structurally diverse mixed-ligand complexes with improved optical, electrochemical, and thermal properties, rendering them promising candidates for advanced applications in catalysis, sensing, and optoelectronic materials. Our compounds have good band gap range for wide band gap semiconductors (WBS) [24]. The thermal study reveals their high temperature thermal stability. The wide band gap materials are more than conventional silicon based semiconductors in some specified uses as they can operate at high temperature, high voltage and high frequency and therefore use in energy transfer electronic devices. The present work is focused on the synthesis, structural characterization and application of some mixed ligand coordination complexes. Formazan and diphenylamine(DPA) used as ligand with variable transition metals. Formazans and their transition metal complexes have been extensively explored over the past decades in versatile applications. Herein the prepared metal complexes explored as potential indirect bandgap semiconductor, catalyst and sensitizer for optoelectronic devices specifically photodetector.

2. Experimental Section

Unless otherwise indicated, all the chemicals and solvents of Analytical grade were obtained from commercial suppliers and used without further purification.

Preparation of 1-(p-nitrophenyl)-3-(o-hydroxyphenyl)-5-phenyl formazan(L-1)

(a) (E)-2-((2-phenylhydrazineylidene)methyl)phenol

20 mmol of salicylaldehyde and 20 mmol of phenylhydrazine hydrochloride were taken in 30 mL 10% acetic acid. The reaction mixture was kept on stirring for 1 hour at room temperature. The dirty white precipitation has appeared and reaction mixture was further stirred for 40 min. The precipitate was filtered off and washed with cold water. Melting point: 140ºC. Yield: 72%.

^{1}H-NMR(300MHz): Chemical Shift(in ppm):10.8(s,1H), 7.86(S,1H), 7.49(S,1H), 7.29(t, 2H), 7.22(d, 1H), 7.14(d, 1H), 6.98(m, 3H), 9.91(dd, 2H).

(b) Diazotization of 4-nitroaniline

0.70g 4-nitroaniline was taken in 10 mL 50% aq. HCl and 0.34 g $NaNO_2$ was dissolved in water and solution kept at 0ºC. The acidic Solution of 4-nitroaniline was added drop wise in $NaNO_2$ with continuous stirring at 0ºC. After complete addition the mixture was further stirred for 1 hour to get diazotized product.

(c) Preparation of 1-(p-nitrophenyl)-3-(o-hydroxyphenyl)-5-phenyl formazan

1.0 g (E)-2-((2-phenylhydrazineylidene)methyl)phenol in 15 ml pyridine was taken in Round bottom flask and freshly prepared 4-nitrobenzenediazoium chloride was dropwise added to it. The temperature was kept between 10-15ºC and the reaction mixture was kept on stirring for 2-3 hrs. Chocolate coloured sticky pricipitate appears. The reaction mixture was poured in to ice-cold water. The sticky product has separated out. The product was filtered and washed with water followed by cold methanol. Yield:- 58%.

1H-NMR (300MHz): Chemical Shift(ppm)- 14.68(S, 1H), 10.69(S, 1H), 8.27(d, 2H), 8.17(d, 2H), 7.95(m,), 7.81(t, 1H), 7.61(d,), 7.31(m), 7.14(s, 1H), 7.02(m, 1H), 6.92(d, 1H).

Synthesis of Diphenylamine formazan metal complexes

$[Co_2(Fz)_2(NPh_2)_2]$ complex

Aqueous solution of 4 mmol of $CoCl_2.6H_2O$ was taken in R.B flask. An ethanolic solution of 8 mmol formazan(L-1) was added dropwise in metal salt solution with stirring. 8 mmol diphenyl amine(DPA) followed by 5 ml 0.1M aq. NaOH was added in the reaction mixture. After 2 hrs stirring purple colour appeared and after 3 hrs stirring merlot red coloured precipitate appeared. The reaction mixture was left overnight at 0ºC, precipitate was appeared. The compound was filtered and washed with cold ethanol. Melting Point : >300ºC.

1H-NMR(300MHz): The complex has paramagnetic character so due to paramagnetic coupling spectra was not clear.

$[Fe_2(Fz)_2(NPh_2)_2]$ complex

A mixture of formazan (L-1), diphenylamine(DPA), and ferric chloride in a 2:2:1 molar ratio was prepared. 20 mL of ethanol was added to the mixture, and it was heated to reflux for 25 minutes. The mixture was then cooled and stirred for 2 hours at room temperature. The reaction mixture was kept on standing at room temperature for 30 min, a precipitate was appeared. The precipitate was filtered and washed with cold ethanol and water in ration 1:1.

1H-NMR (300MHz): Only few signals are clear but the proton attached to nitrogen peak was disappear. Which confirm the formation of complex.

$[Cu_2(Fz)_2(NPh_2)_2]$ complex

Cupric acetate, diphenylamine(DPA), and formazan(L-1) were taken in a ratio of 1:2:2 in a round-bottom flask, and 20 ml of methanol was added to the mixture. The reaction mixture was heated to reflux for 2.5 hours and then left at room temperature for 1-2 hours. A greenish-black precipitate was observed. The reaction mixture was filtered and washed with cold methanol.

1H-NMR (300MHz): No peaks was appears due to paramagnetic coupling.

3. Characterization

^{1}H-NMR for prepared compound were recorded at 300MHz in $CDCl_3$ at room temperature (Model-ECZ-500R). FT-IR emission spectra were recorded by ATR method using FT-IR spectrometer (FT-IR 4700 JASCO). UV-Vis absorption Spectra were recorded by UV-Vis NIR spectrophotometer in solid state/liquid state. Current voltage relation and Impedance measurement done by solar simulator (MULTI AUTOLAB M204) electrochemical work station.

4. Result and discussion

The 1-(p-nitrophenyl)-3-(o-hydroxyphenyl)-5-phenylformazan(L-1) ligand was prepared by coupling of diazonium salt of 4-nitroaniline and (E)-2-((2-phenylhydrazineylidene)methyl)phenol (Schiff base)[25]. The scheme involved are shown in scheme-1. Tranisition metal bimetallic complexes with ligand 1-(p-nitrophenyl)-3-(o-hydroxyphenyl)-5-phenylformazan (L-1) and diphenyl amine were prepared and characterized by spectroscopic methods.

4.1 Elemental analysis

- The percentage composition of elements in metal complexes were characterized by CHNS Analyzer (Elementar Vario EL Cube) whereas metal content were estimated by gravimetric analysis. From the elemental composition (table-1) the simple ratio in metal, ligand L-1 and Diphenyl amine are 1:1:1. Molecular formula of complex was $[M_2(Fz)_2(NPh_2)_2]$(M = Co(II)/Fe(II)/Cu(II)).

Table-1

Elemental analysis of metal complexes.

S. No.	Complex	Molecular Weight	%C	%H	%N	%O	%M
1.	**$[Co_2(Fz)_2(NPh_2)_2]$**	**1176**	**63.26**	**4.42**	**14.28**	**8.16**	**10.03**
2.	$[Fe_2(Fz)_2(NPh_2)_2]$	1171	63.5	4.44	14.34	8.19	10.07
3.	$[Cu_2(Fz)_2(NPh_2)_2]$	1185	62.78	4.38	14.17	8.10	9.95

4.2 Spectroscopic Analysis

The complex were analysed using various spectroscopic methods. The FT-IR spectra of 1-(p-nitrophenyl)-3-(o-hydroxyphenyl)-5-phenyl formazan (L-1) and metal complexes are in figure-2 and comparative data shown in table-2. The IR frequencies in metal complexes are slightly decreases than the ligand L-1. –N-H stretching band disappears which indicates the ligand bind in formazonate form. Also diphenylamine binds in deprotonated form. O-H stretching band also disappears in metal complexes and weak in L-1 which is probably due to hydrogen bonding.

Table-2

FT-IR data for ligand (L-1) and metal complexes.

S. No.	Bonds	Vibrational frequencies (cm^{-1})			
		Formazan	$[Co_2(Fz)_2(NPh_2)_2]$	$[Fe_2(Fz)_2(NPh_2)_2]$	$[Cu_2(Fz)_2(NPh_2)_2]$
1.	O-H	3780	3443	3477	3484
2.	N-H	3690	---	----	---
3.	^{sp2}C-H	3100(w)	2890	3060	3070
4.	-C = N-	1604	1590	1590	1600
5.	-N = N-	1566	1576	1524	1508
6.	-C-N-	1360	1342	1345	1340
7.	$(-C = C-)_{arm}$	1520 – 1430	1512 – 1383	1510 – 1380	1390
8.	-N = O	1320	1306	1233	1236
9.	$-C-O_{phenolic}$	1240	1245		1184

The ^{1}H-NMR data were shown in experimental section and ^{1}H-NMR plot were shown in supplementary data. ^{1}H-NMR spectra of metal complexes are broadened and the signals are clearly not identified probably due to paramagnetic coupling [26].

4.3 UV-Vis spectra

UV–visible absorption spectroscopy is an important technique for investigating the optical and electronic properties of materials. It provides valuable information regarding band-gap energies, electronic transitions, and molecular interactions within a system [27].

The position and intensity of absorption bands are associated with specific electronic transitions and reflect the electronic structure of the compounds [28]. Organic molecules have the absorption bands specifically corresponds to π→π* and n→π* transitions. But in coordination complexes, the spectra are usually more complex due to the presence of d–d transitions, charge-transfer (CT) transitions, and inter-ligand charge-transfer (ILCT) processes, which pointedly impact on their optical behavior. The λ_{max} for ligand(L-1), complexes of Co(III) and Fe(III) are 417nm, 418nm and 401 nm respectively(fig.-2). These λ_{max} values for ligand are due to n→π* transition where as in metal complexes it is due to charge transfer. The same transition were appeared for Fe(II) and Co(II) complexes but intensity were different [29]. Another transition in UV-vis spectra are observed around 295 nm in each compound due to interligand charge transfer or π→π*. The λ_{max} for Cu(II) was 303.4nm corresponds to d-d transition or

LMCT, absorbance for Cu(II) are not good and it is drop from ligand. Relatively large band gap for Cu(II) causes low wavelength.

4.4 Thermo-gravimetric analysis

The thermogravimetric analysis (TGA) profiles of Metal complexes $[Co_2(Fz)_2(NPh_2)_2]$, $[Fe_2(Fz)_2(NPh_2)_2]$ and $[Cu_2(Fz)_2(NPh_2)_2]$ reveal their thermal stability and decomposition behavior over the temperature range of 0–500°C. The thermograms for the complexes given in supplementary data. All complexes exhibit an initial minor weight loss below ~ 120°C, which can be credited to the removal of moisture. A stable plane is observed up to ~ 200–250°C, indicating good thermal strength of the complexes. The major decomposition step occurs in the range of ~ 250–400°C, corresponding to the breakdown of the organic ligand framework. Among the complexes $[Cu_2(Fz)_2(NPh_2)_2]$ shows comparatively higher thermal stability with a steady weight loss, suggesting stronger metal–ligand coordination. $[Fe_2(Fz)_2(NPh_2)_2]$ displays a slightly earlier onset of decomposition, indicating relatively lower stability. Whereas $[Co_2(Fz)_2(NPh_2)_2]$ demonstrates intermediate behavior between these two complexes. All three complexes are appreciable thermally stable, making them suitable at high temperature optoelectronics and semiconductor applications.

4.5 Optical band gap

The optical band gap for formazan and complexes was calculated by applying tauc plot method [27]. Value of optical band gap was obtained by extrapolation of the linear region to zero absorbance from the plot that was drawn according to the tauc relation.

$(\alpha h\upsilon)^n = (h\upsilon - E_g)$, n= ½ for indirect band gap

n = 2; direct band gap

Where, α is absorbance, E_g is band gap, and hυ is absorbed photon energy.

The plot of $(\alpha h\upsilon)^{1/2}$ vs hυ were shown in figure-3 and the band gap calculated via extra polating linear part of curve at energy axis. The energy gap calculated for the complexes are shown in table-2. The band gap for complexes are > 2 eV corresponds to indirect transition i.e; these complexes are considered as potential wide band gap semiconductors for optoelectronic applications.

Table-3

Maximum wavelength and corresponding energy gap.

S. No.	Compounds	λ_{max}	Energy gap (eV)
1.	1-(p-nitrophenyl)-3-(o-hydroxyphenyl)-5-phenyl formazan (Fz) [L-1]	418 nm	2.24
2.	$[Co_2(Fz)_2(NPh_2)_2]$	400.7 nm	2.37
3.	$[Fe_2(Fz)_2(NPh_2)_2]$	401.32 nm	2.62
4.	$[Fe_2(Fz)_2(NPh_2)_2]$	303.4 nm	2.89

4.6 Electrochemical impedance spectroscopy (EIS) Study

Electrochemical impedance spectroscopy measurement were carried out under open light to evaluate the charge transport and charge recombination behaviour of DSSCs over the wide frequency ranges from 0.1 Hz to 10 kHZ. The EIS parameters for assembled cells are shown

in table-4. The bode impedance plot shows high impedance at low frequency region due to electron recombination at dye-electrolyte interface [30]. At high frequency the continous decreasement in impedance observed which suggests improved charge transport and reduced Polarization loss. The broad phase angle (~ 45ºC-55ºC) Observed at mid frequency region. The characterstics of non-ideal capacitor due to electron accumulation and trap assited transport and surface roughness within TiO_2 photoanode, the broad phase angle suggest the distributed relaxation process [31].

Table-4

EIS parameter of DSSCs fabricated using different dye.

Cell	Voc (V)	R_s (Ω)	R_{CT}	n	CPE $S*s^n$	Lifetime
Cell-1	1.98	110	5.34 kΩ	0.696	37.9	10.6–3.18 mS
Cell-2	1.97	201	7.62 kΩ	0.874	17.2	7.8–3.9 mS
Cell-2	1.99	61.1	759 Ω	0.861	21.8	3.18–1.99 mS

Nquist Plot for each cell displays a single semicircle without Warburg tail. Single semicircle indicating the primary impedance response due to charge transfer and interfacial polarization.[32] The absence of other semicircle corresponds to photoanode/ electrolyte suggests that the recombination process totally governed by impedance behaviour. The experimental data were well fitted via equivalent circuit model and CPE parameter were evaluated.

Table-5: Equivalent circuit model for fabricated DSSCs.

S. No.	Cell	Voc(volt)	Circuit diagram
1.	Cell-1	1.98	
2.	Cell-2	1.97	
3.	Cell-2	1.99	

Where the series ressistance ranges from 65Ω − 200Ω due to ITO substrate. Relatively high charge transfer resistance indicates suppressed electron recombination which is better for achieving higher open circuit voltage. The CPE parameters (n < 1) for cells indicates deviation from ideal capacitive behaviour due to non-uniform interfacial charge distribution.

4.7 I-V measurement of fabricated DSSCs

The photovoltaic (I-V) performance of the fabricated cells were analysed under illumination intensity of 100mWcm^{-1} with air mass 1.5 AM filter. The SI figure shows I-V curve for TiO_2 based DSSCs with metal formazonate dyes in dark. The cells have very low (2–10 mAmp) current. The calculated parameters are shown in table-6. The low current materials have potential application as photodetectors [33] and cathodic current suggest applications in hydroden evolution reaction [34]. Which were due to high resistance and suppressed charge recombination. Photoconversion efficiency is extremely low. I-V curve analysis suggests cathodic current. Also the Photocurrent and Quantum yield of the cell for visible range are moderate; i.e: 20–70%.

Table-6: Photovoltaic Parameters for DSSC cells as low current applications.

S. No.	Dye	Cell	V_{oc}	J_{sc}	FF	%η
1.	$[Co_2(Fz)_2(NPh_2)_2]$	Cell-1	1.98 V	-4 mA	0.642	< 0.01
2.	$[Fe_2(Fz)_2(NPh_2)_2]$	Cell-2	1.97 V	-10 mA	0.614	< 0.01
3.	$[Cu_2(Fz)_2(NPh_2)_2]$	Cell-3	1.99 V	-9.67 mA	0.282	< 0.01

5. Conclusion

Metal complexes of Fe(II), Co(II), and Cu(II) were synthesized using formazan derivative(L-1) and diphenylamine ligands using an simple and economic approach. These complexes are in a general molecular formula of $[M_2A_2B_2]$, which was confirmed by elemental analysis. The FT-IR and ^{1}H NMR spectroscopy confirms structure of ligands and metal complex preparation. Further thermo-gravimetric analysis revealed that the complexes are thermally stable up to 300°C without any significant degradation in ambient conditions. UV–Vis absorption spectra exhibited intense bands in the visible region, The indirect optical band gaps, calculated from solid-state UV–Vis data using the tauc equation and the bandgap found to be in the range of 2.0–3.0 eV. Which indicates their suitability for photovoltaic

applications with variable temperature range. The photocurrents in cells are 10–20 mA range, which were not suitable for Solar cell due to low cathodic photo current of the prepared materials. These compounds have potential application in photo-diode detectors for visible region, indoor photovoltaic device and also useful in hydrogen generation reactions. Overall, the synthesized metal–formazan complexes exhibit favourable optical, thermal, and photovoltaic properties.

Declarations

Competing interest

The author declare that they have no competing interest.

Author Contribution

Pravendra kumar and Sushmita Gupta conceptualised the work. Pravendra Kumar wrote the manuscript text and data analysis. Brijesh Kumar did data curation and manuscript corrections. All the authors reviewed the manuscript.

Acknowledgements

One of the author (**Pravendra Kumar**) acknowledges the financial support of CSIR-UGC JRF **(File No. 09/0522/15658/2022/ EMR-I)** programme under the MoE, Govenrment of india.

References

1. Thwaites PA, Yao CK, Halmos EP, Muir JG, Burgell RE, Berean KJ, Kourosh Kalantar-zadeh, Gibson PR (2024) Review Article: Current Status and Future Directions of Ingestible Electronic Devices in Gastroenterology. *Alimentary Pharmacology & Therapeutics 4*. https://doi.org/10.1111/apt.17844
2. Fan P, Chettiar UK, Cao L, Afshinmanesh F, Engheta N, Brongersma ML (2012) An Invisible Metal–Semiconductor Photodetector. Nat Photonics 6(6):380–385. https://doi.org/10.1038/nphoton.2012.108
3. Ma T, Xue N, Muhammad A, Fang G, Yan J, Chen R, Sun J, Sun X (2024) Recent Progress in Photodetectors: From Materials to Structures and Applications. Micromachines 15(10):1249. https://doi.org/10.3390/mi15101249
4. Bahram Nabet (2016) Photodetectors: Materials, Devices and Applications. Woodhead Publishing, Cambridge
5. Baeg K-J, Binda M, Natali D, Caironi M, Noh Y-Y (2013) Organic Light Detectors: Photodiodes and Phototransistors. Adv Mater 25(31):4267–4295. https://doi.org/10.1002/adma.201204979

6. Marouf H, Nariman A-S, El-Rabaie E-SM, Nabih A, ElKhamisy KM (2025) A Comprehensive Review of Photodetectors: Materials, Enhancement Techniques, Perspectives, and Recent Directions. J Opt. https://doi.org/10.1007/s12596-025-02779-4
7. Fu J, Nie C, Sun F, Li G, Wei X (2023) Photodetectors Based on Graphene–Semiconductor Hybrid Structures: Recent Progress and Future Outlook. *Advanced Devices & Instrumentation 4*. https://doi.org/10.34133/adi.0031
8. Nalwa HS (2020) A Review of Molybdenum Disulfide (MoS2) Based Photodetectors: From Ultra-Broadband, Self-Powered to Flexible Devices. RSC Adv 10(51):30529–30602. https://doi.org/10.1039/d0ra03183f
9. Chen J, Li M, Lin H, Zhou C, Chen W, Wang Z, Li H (2025) Advances in One-Dimensional Metal Sulfide Nanostructure-Based Photodetectors with Different Compositions. J Compos Sci 9(6):262–262. https://doi.org/10.3390/jcs9060262
10. Fan M-M, Cao L, Xu K-L, Li X-Y (2020) Mixed-Phase β-Ga2O3 and SnO2 Metal-Semiconductor-Metal Photodetectors with Extended Detection Range from 293 Nm to 330 Nm. J Alloys Compd 853:157080–157080. https://doi.org/10.1016/j.jallcom.2020.157080
11. Sun S, Li W, Zhang Y, Gao Q, Zhang N, Qin Y, Feng W (2024) Mixed Metal Oxide Heterojunction for High-Performance Self-Powered Ultraviolet Photodetection. *Small* https://doi.org/10.1002/smll.202407107
12. Nineham AW (1955) The Chemistry of Formazans and Tetrazolium Salts. Chem Rev 55(2):355–483. https://doi.org/10.1021/cr50002a004
13. Shawali AS, Samy NA (2015) Functionalized Formazans: A Review on Recent Progress in Their Pharmacological Activities. J Adv Res 6(3):241–254. https://doi.org/10.1016/j.jare.2014.07.001
14. Moussa SH, Tayel AA, Al-Hassan AA, Farouk A (2013) Tetrazolium/Formazan Test as an Efficient Method to Determine Fungal Chitosan Antimicrobial Activity. *Journal of Mycology 2013*, 1–7. https://doi.org/10.1155/2013/753692
15. DeRosa TF, Formazan (2006) *Advances in Synthetic Organic Chemistry and Methods Reported in US Patents* 272–274. https://doi.org/10.1016/b978-008044474-1/50034-7
16. Ghadhban FS, Kadhim MI, Preparation (2022) Spectroscopic and Biological Study of Some Derivatives of Formazan and New Heterocyclic Compounds. Int J health Sci 7337–7344. https://doi.org/10.53730/ijhs.v6ns4.10465
17. Gilroy JB, Otten E (2020) Formazanate Coordination Compounds: Synthesis, Reactivity, and Applications. Chem Soc Rev 49(1):85–113. https://doi.org/10.1039/C9CS00676A
18. Mariappan G, Korim R, Joshi N, Alam F, Hazarika R, Kumar D, Uriah T (2010) Synthesis and Biological Evaluation of Formazan Derivatives. J Adv Pharm Tech Res 1(4):396. https://doi.org/10.4103/0110-5558.76438
19. Palatanchirakkal R, Chennikkad R, Kavitha AP, Farhan KM, Bijudas K, Andikkadankuzhiyil AR, Tharayil SB, Synthesis (2025) Characterization, and Biological Evaluation of 3-Benzoyl-1,5-Di-(4-

Bromophenyl) Formazan and Its Metal Complexes: Structural Insights and Antibacterial Activity. J Mol Liq 428:127545. https://doi.org/10.1016/j.molliq.2025.127545

20. Shakeel AK, Rizwan K, Shahid S, Noamaan MA, Rasheed T, Amjad H, Synthesis DFT (2020) Computational Exploration of Chemical Reactivity, Molecular Docking Studies of Novel Formazan Metal Complexes and Their Biological Applications. Appl Organomet Chem 34(3). https://doi.org/10.1002/aoc.5444
21. Capulín Flores L, Mondria SJ, Kuessner K-T, Rohatschek P, Siewert I, Zúñiga-Villarreal N, Otten E (2025) Synthesis and Electrochemistry of Formazan(Ate) Re(I) Complexes: Ligand-Based Reactivity toward CO_2. Inorg Chem 64(43):21603–21619. https://doi.org/10.1021/acs.inorgchem.5c03626
22. Wang D, Dong H, Wu Y, Yu Y, Zhou G, Li L, Wu Z, Gao M, Wang G Effect of Diphenylamine Substituent on Charge-Transfer Absorption Features of the Iridium Complexes and Application in Dye-Sensitized Solar Cell, Rodriguez MA, Bunge SD, Diphenylamine (eds) (2015) *Journal of Organometallic Chemistry 775*, 55–59. https://doi.org/10.1016/j.jorganchem.2014.10.031. (b). Rodriguez MA, Bunge SD, Diphenylamine. *Acta Crystallographica Section E: Structure Reports Online* 2003, *59* (8), o1123–o1125. https://doi.org/10.1107/S1600536803014788
23. Wortmann S, Kutta RJ, Nuernberger P (2022) Monitoring the Photochemistry of a Formazan over 15 Orders of Magnitude in Time. Front Chem 10:983342–983342. https://doi.org/10.3389/fchem.2022.983342
24. Omar Sarwar Chaudhary, Mouloud Denaï, Refaat SS (2023) Georgios Pissanidis. Technology and Applications of Wide Bandgap Semiconductor Materials: Current State and Future Trends. Energies 16(18):6689–6689. https://doi.org/10.3390/en16186689
25. Turkoglu G, Berber H (2016) Novel Formazan Derivatives Containing Phenylsulfanyl and Carbonyl Units: Synthesis, Optical and Electrochemical Properties. RSC Adv 6(98):96065–96078. https://doi.org/10.1039/c6ra23008c
26. Novotny J, Stanislav K, Marek R (2024) Paramagnetic Effects in NMR Spectroscopy of Transition-Metal Complexes: Principles and Chemical Concepts. Acc Chem Res 57(10). https://doi.org/10.1021/acs.accounts.3c00786
27. Makuła P, Pacia M, Macyk W (2018) How to Correctly Determine the Band Gap Energy of Modified Semiconductor Photocatalysts Based on UV–Vis Spectra. J Phys Chem Lett 9(23):6814–6817. https://doi.org/10.1021/acs.jpclett.8b02892
28. Bertoloni RR, Ramos VM, de Lima Batista AP, de Oliveira-Filho AGS (2025) Benchmarking Structures and UV–Vis Spectra of Iron Complexes against Experimental Data. J Phys Chem A 129(45):10481–10495. https://doi.org/10.1021/acs.jpca.5c06391
29. Vinusha HM, Kollur SP, Revanasiddappa HD, Ramu R, Shirahatti PS, Nagendra Prasad MN, Chandrashekar S, Begum M, Preparation (2019) Spectral Characterization and Biological Applications of Schiff Base Ligand and Its Transition Metal Complexes. Results Chem 1:100012. https://doi.org/10.1016/j.rechem.2019.100012

30. Liberatore M, Decker F, Burtone L, Zardetto V, Brown TM, Reale A, Di Carlo A (2009) Using EIS for Diagnosis of Dye-Sensitized Solar Cells Performance. J Appl Electrochem 39(11):2291–2295. https://doi.org/10.1007/s10800-009-9806-5
31. Mei B-A, Munteshari O, Lau J, Dunn B, Pilon L (2017) Physical Interpretations of Nyquist Plots for EDLC Electrodes and Devices. J Phys Chem C 122(1):194–206. https://doi.org/10.1021/acs.jpcc.7b10582
32. Allison A, Andreas HA (2019) Minimizing the Nyquist-Plot Semi-Circle of Pseudocapacitive Manganese Oxides through Modification of the Oxide-Substrate Interface Resistance. J Power Sources 426:93–96. https://doi.org/10.1016/j.jpowsour.2019.04.029
33. Su C, Li M, Yan H, Zhang Y, Li H, Fan W, Bai W, Liu X, Wang Q, Yin S (2025) $PdSe_2$/$NbSe_2$ Heterojunction Photodetector with Broadband Detection and Polarization Sensitivity. ACS Appl Mater Interfaces 17(3):5213–5222. https://doi.org/10.1021/acsami.4c17285
34. Xu Y, Yu S, Zhu Y-C, Fan G-C, Han D, Qu P, Zhao W-W (2019) Cathodic Photoelectrochemical Bioanalysis. *trac-trends*-in-*analytical-chemistry 114*, 81–88. https://doi.org/10.1016/j.trac.2019.03.002

Scheme

Scheme 1 and 2 is available in the Supplementary Files section.

Figures

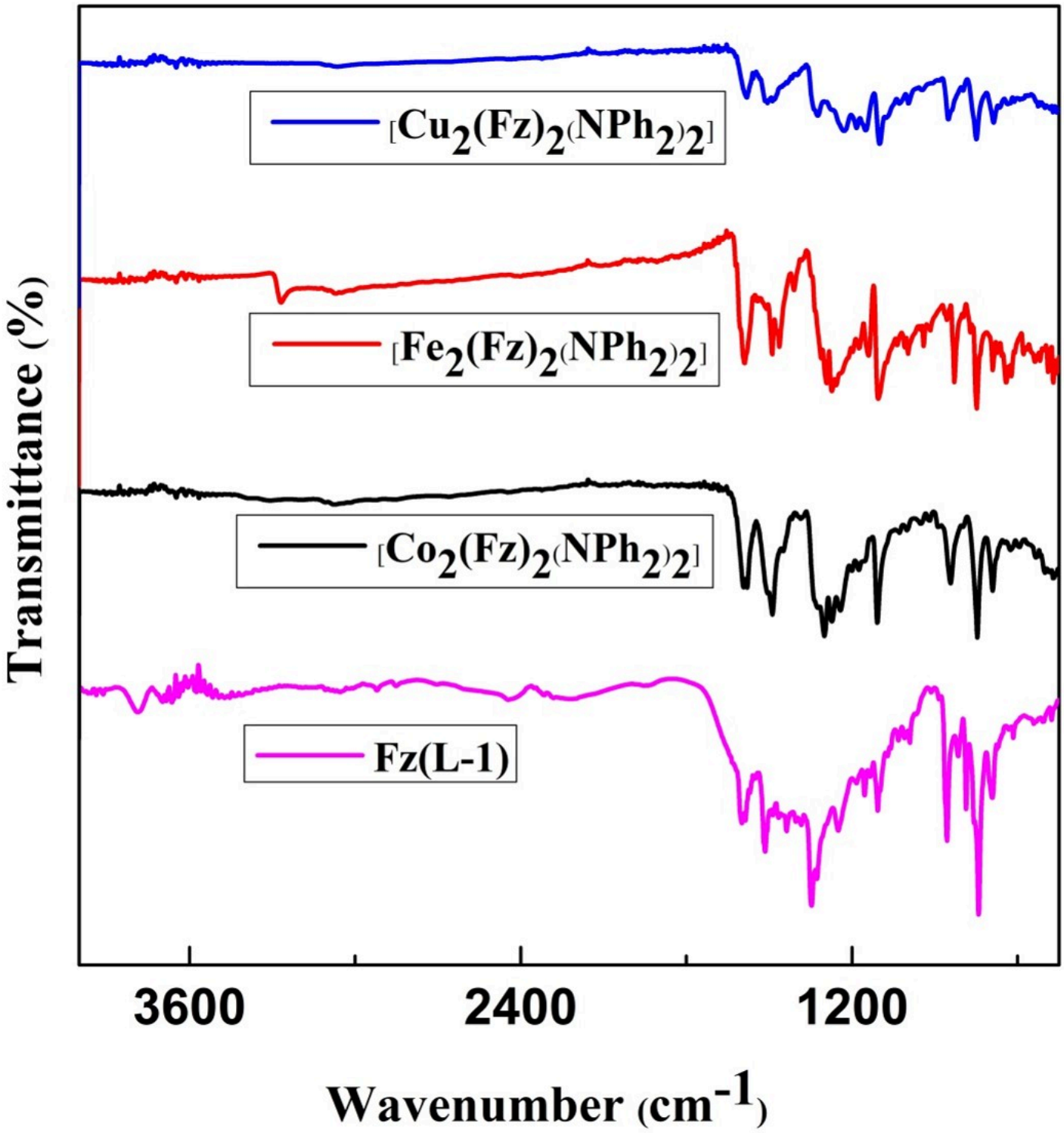


Figure 1

FT-IR spectra of complexes and formazan(L-1**).**

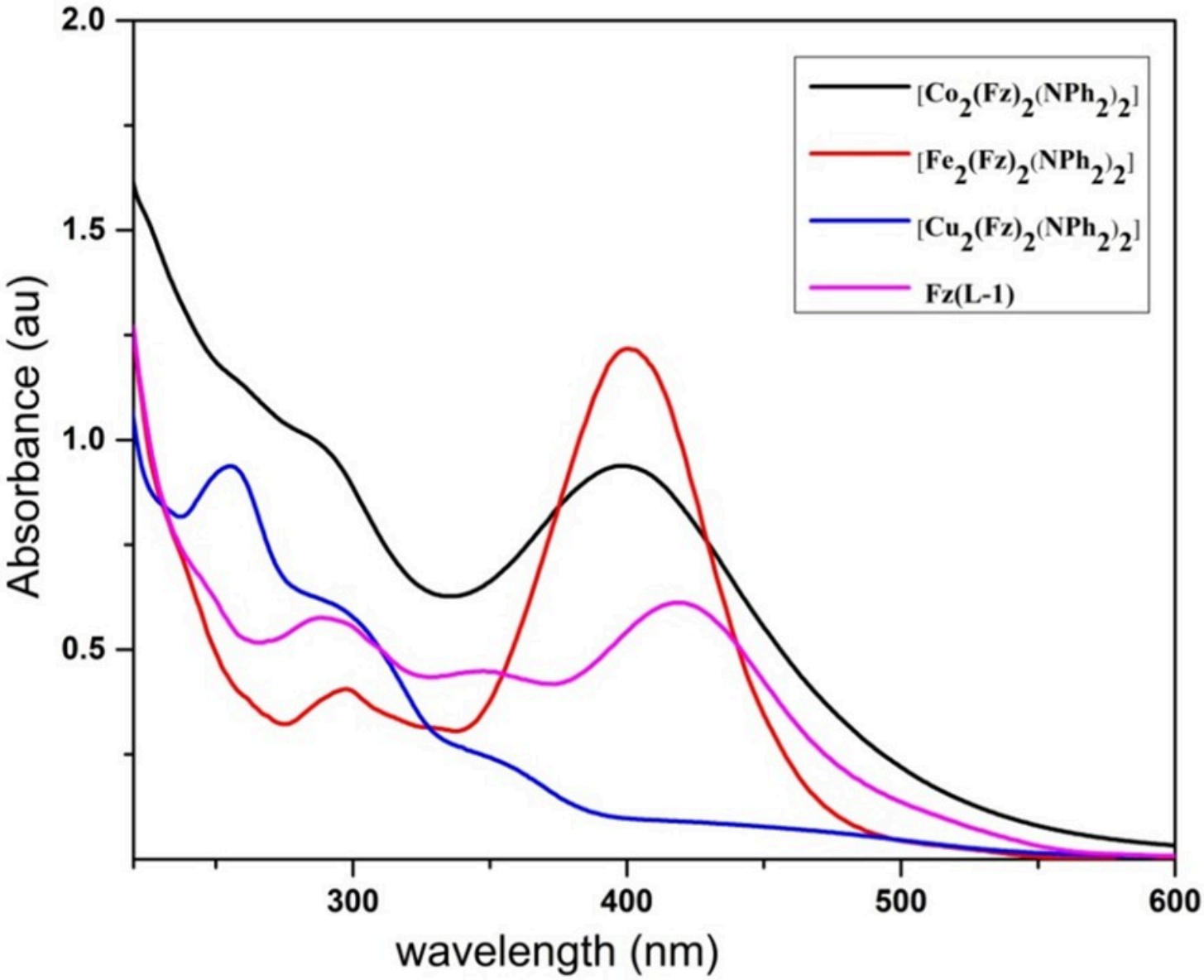


Figure 2

UV-Vis Spectra of ligand L-1 and metal complexes.

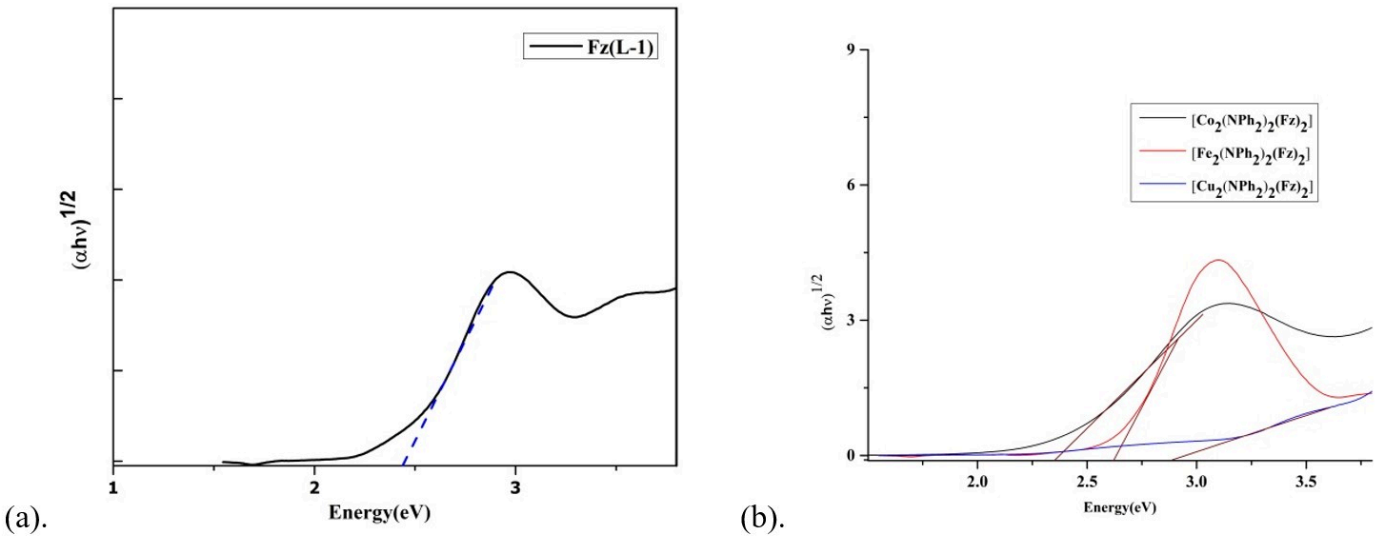


Figure 3

Tauc Plot of (a) Farmazan (L-1). (b) $[Co(Fz)_2(NPh_2)_2]$, $[Fe(Fz)_2(NPh_2)_2]$ and $[Cu(Fz)_2(NPh_2)_2]$.

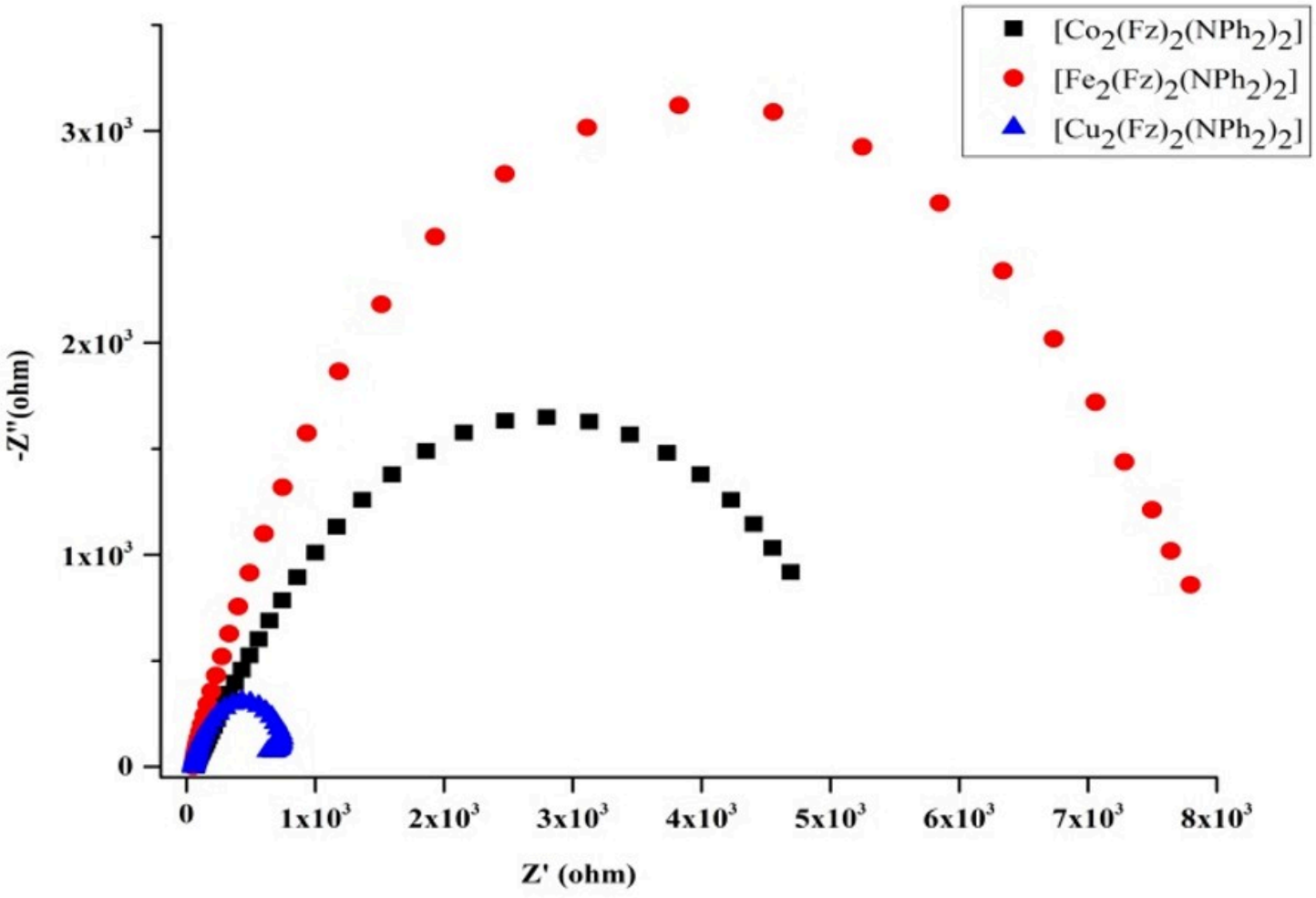


Figure 4

Nquist Plot of different metal complexes.

Supplementary Files

This is a list of supplementary files associated with this preprint. Click to download.

- SupplementryInformation.docx
- Scheme.docx